ACS OMEGA

http://pubs.acs.org/journal/acsodf

Article

Synthesis of Chitosan-Silver Nanocomposite and Its Evaluation as an Antibacterial Coating for Mobile Phone Glass Protectors

Gibson Jake C. Canama, Monica Claire L. Delco, Rhoel A. Talandron, and Noel Peter Tan*

Cite This: *ACS Omega* 2023, 8, 17699−17711

Read Online

ACCESS | Metrics & More | Article Recommendations

ABSTRACT: An easy and environment-friendly route for antibacterial coating suited for mobile phone glass protectors was successfully demonstrated. In this route, freshly prepared chitosan solution in 1% v/v acetic acid was added with 0.1 M silver nitrate solution and 0.1 M sodium hydroxide solution and incubated with agitation at 70 °C to form chitosan-silver nanoparticles (ChAgNPs). Varied concentrations of chitosan solution (i.e., 0.1, 0.2, 0.4, 0.6, and 0.8% w/v) were used to investigate its particle size, size distribution, and later on, its antibacterial activity. Transmission electron microscope (TEM) imaging revealed that the smallest average diameter of silver nanoparticles (AgNPs) was 13.04 nm from 0.8% w/v chitosan solution. Further characterizations of the optimal nanocomposite formulation using UV−vis spectroscopy and Fourier transfer infrared spectroscopy were also performed. Using a dynamic light scattering zetasizer, the average ζ-potential of the optimal ChAgNP formulation was at +56.07 mV, showing high aggregative stability and an average ChAgNP size of 182.37 nm. The ChAgNP nanocoating on glass protectors shows antibacterial activity against *Escherichia coli* (E. coli) at 24 and 48 h of contact. However, the antibacterial activity decreased from 49.80% (24 h) to 32.60% (48 h).

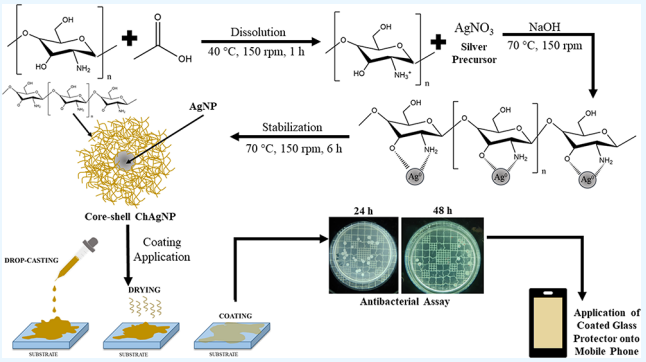

1. INTRODUCTION

Bacterial infections are a globally concerning issue affecting health and safety, morbidity, and mortality. These infections can be transmitted through inanimate objects or gadgets that carry bacteria and viruses. One of these indispensable gadgets is mobile phones, which have a high-touch surface and can be a reservoir of disease-causing microorganisms and, thus, a high-potential source of transmission.[1,2]

The growing role of mobile phones in causing bacterial and viral infections is alarming. For example, a study showed that about 91.7% of 192 swabbed mobile phones showed bacterial contamination in a community setting.[1] On the other hand, 62.0% of 400 tapped mobile phones from varied communities such as schools, food stalls, public offices, and hospitals showed bacterial contamination, with food vendors having the highest contamination rate.[2] A review in the hospital reported that 10−100% of mobile phones sampled were contaminated according to 39 studies worldwide, including countries such as India, Nigeria, and the United States, among others, between 2005 and 2013, totaling 4876 samples.[3] *Staphylococcus aureus* (*S. aureus*) was cited as the most prevalent bacterial species found on the mobile phone surface in both community and hospital settings. *Escherichia coli* (*E. coli*) is also among those found in both settings. These pathogens, if not disinfected, can permeate dry surfaces for several months.[4]

Disinfection is one of the measures used to mitigate these microorganisms' spread on surfaces and decrease such contamination. Several strategies with various pathogen-killing formulations have been studied for their disinfection properties. The most popular tools and technologies for electronic gadget disinfection devices include sanitizer sprays, self-cleaning coatings, disinfectant wipes, and even UV light sanitizing devices. The use of alcohol and alcohol-based disinfectants has excellent potential to kill bacteria and viruses on human skin. The antibacterial mode of action of alcohols is done by the denaturation of proteins found in bacteria.[5] Furthermore, around 70% alcohol concentration suffices in disinfecting electronic devices.

Another disinfection alternative is the use of self-cleaning protectors for mobile phones. These screen protectors can come as plastic films or as tempered glass. Screen protectors are applied to mobile phones to save costs from repairing broken screens and improving screen durability.[6] One of the

Received: January 10, 2023
Accepted: April 26, 2023
Published: May 10, 2023

most widely used screen protectors for mobile phones is the tempered glass type due to its durability, scratch resistance, and embedded antifingerprint technology. Aside from enhancing mobile phone mechanical properties, screen protectors are used to disinfect gadgets by incorporating antibacterial and antiviral coatings. The most commonly used coating materials are titanium dioxide (TiO_2) photocatalytic (or light-activated) coating, copper-based coating, reactive oxygen species (ROS)-based coating, and quaternary-ammonium compounds (QACs). These coatings are embedded or applied onto screen protectors, which may come as plastic film or tempered glass. While there have been available commercial self-cleaning glass protectors, they showed little to no effect on their antibacterial activity. Titanium dioxide is used as a coating on surfaces in intensive care units and was observed to not affect microbial colonization on such surfaces.[7] QAC, on the other hand, induces a rapid decrease in the bacterial count only after 72 h. Consequently, excess or deficiency of the copper-based material can be lethal and hard to clean.[7−9]

One of the sought-after nanoparticles with antibacterial properties are silver nanoparticles (AgNPs). Compared to other metal nanoparticles, AgNPs are better in antibacterial activity and stability. AgNPs are much-favored metal nanoparticles due to their higher antibacterial activity compared to other metal nanoparticles with fewer oxidation aftermaths.[10,11]

Investigations have shown that silver nanoparticles exhibit antibacterial activity against Gram-negative and Gram-positive bacteria. Among them include *Staphylococcus aureus* (*S. aureus*), *Escherichia coli* (*E. coli*), *Candida albicans*,[12,13] *Klebsiella pneumoniae* (*K. pneumoniae*),[13] multiple antibiotic-resistant (MAR) *Klebsiella pneumoniae*,[14] *Enterococcus faecium*, *Pseudomonas aeruginosa*, and *Staphylococcus epidermis*.[13]

Unlike other chemical agents, such as borohydrides and hydrazine, which are detrimental to the environment and health, green reagents are used to reduce risks.[15] Toxic-reducing reagents have often been utilized in the chemical synthesis of metal nanoparticles, making them impractical for biomedical applications.[16]

The applications of silver nanoparticles have brought about numerous innovations, such as in medical instruments, infant products, cosmetics, and food coatings, including using these nanoparticles on glass surfaces.[17] The study of Hofmeister et al. noted the stability of AgNPs embedded in glass under various fabrication techniques.[18] Pallavicini et al. assessed the antibacterial activity of AgNPs on glass. Nanoparticles were found firmly grafted onto the glass surface even after four weeks.[19]

A decimal-log reduction rate of 4.93 against *E. coli* was achieved after 5 h of contact with the AgNPs, while the identical particles obtained a rate of 5.54 against *S. aureus* after 24 h.[19] By European Standard EN 13697, an acceptable microbicidal activity is a decimal-log reduction rate of at least 4 after 5 min of contact.

However, one of the challenges in the use of nanoparticles is the selection of a suitable reagent and other auxiliaries in consideration of environmental friendliness and low toxicity.[20] One of the ways in the metal-ion reduction process is by using biocompatible and environment-friendly biopolymers that can be extracted from natural resources.[20]

On the other hand, biological approaches are preferred to overcome drawbacks such as excessive cost and environmental and biological hazards posed by using toxic, hazardous chemicals from the chemical and physical synthesis of AgNPs.[21]

One novel biological approach is the use of a natural polysaccharide, chitosan. This biopolymer is often used to reduce metal nanoparticles and does not introduce environmentally toxic and biological hazards.[22] Several studies have reported chitosan as an effective reducing reagent in synthesizing silver and gold nanoparticles.[16,22,23] In the presence of chitosan, the reduction of Ag^+ ions to Ag^0 can occur at room temperature owing to the free electron provided by the oxidation of alcohol or glucoside groups in the chitosan molecule. Furthermore, when the reaction temperature is increased, the reduction reaction occurs faster.[16] Many studies have confirmed the application of chitosan-silver nanocomposites (ChAgNPs) in food coatings, antimicrobial coatings, packaging, and other applications.[24−29] Studies have shown that chitosan can be used as a multifunctional template as both a reducing agent and a stabilizing agent in synthesizing the chitosan-silver nanocomposite. Such a multifunctional template is possible due to carbohydrate and amino group polymers acting as reducing and stabilizing agents for metal nanoparticles.[12,30,31] This polysaccharide chitosan is an attractive template for metal nanoparticles because of its availability, biocompatibility, and highly positive charge.

Although chitosan is known for its metal nanoparticle ability to reduce and stabilize metal ions to nanoparticles, there are limited studies observing the relationship between chitosan concentration and AgNP size. It is essential to know such a correlation as it affects the stability and the risk of aggregation depending on the agent used in the nanocomposite synthesis. This preserves the nanostructure properties such as morphology and composition and, in turn, its efficiency upon application. The group of Venkatesham et al. observed that the absorbance value at the 420 nm wavelength peak increases as the concentration of chitosan increases, indicative of the increased efficiency in nanoparticle synthesis.[32] The study of Nate et al. shows the synthesis of ChAgNPs that occurs at 0.5, 1.0, and 2.0% w/v chitosan concentrations. TEM reveals that the smallest average nanoparticle size was measured at 2 nm, using 2.0% w/v chitosan concentration.[23] Thus, chitosan concentration can contribute to the generation of smaller nanoparticle sizes.

In connection, size can affect the antibacterial activity of the nanocomposite, wherein decreasing the particle size of the substance results in improved antibacterial properties.[33] Gram-positive bacteria have a cytoplasmic membrane and a cell wall thickness of 20−28 nm. Meanwhile, Gram-negative bacteria have two-cell membranes with 7−8 nm thickness. To strike through the nucleus of the bacteria, a substance as minor as its thickness is required to pass through and damage the bacteria cell, causing the elimination or death of the microorganism.[34] Thus, it is crucial to control the size of the nanoparticle through the synthesis process and the factors that affect such a reaction. The relationship between particle size and antibacterial activity can be seen in the study of Raghupathi et al. on zinc oxide nanoparticles (ZnONPs). It was observed that the recovered viable cells increased as the particle size increased, which suggests that more significant inhibition is significantly observed at tiny nanoparticle sizes.[35] The same phenomenon was observed in the study of Martínez-Castañón et al. for AgNPs with gallic acid as its reducing agent. Results showed that at 7 nm diameter, a poor minimum inhibition concentration (MIC) was observed for *E. coli* and *S. aureus*

https://doi.org/10.1021/acsomega.3c00191
ACS Omega 2023, 8, 17699−17711

bacteria.[33] These studies prove that the smallest possible nanoparticle made in the synthesis is the optimal candidate for antibacterial activity and shall be used for assessment during application. Another factor to consider in assessing the antibacterial activity of nanomaterial coatings is contact time, that is, the duration in which the surface is in contact with the bacteria to kill the latter. It serves as an indicator of the efficacy of the material in being an antibacterial agent.[36] Minimal studies have been made in investigating ChAgNPs as an antibacterial coating on glass surfaces and the contact time needed for it to exhibit microbial activity.

In this study, two objectives were targeted. The first is to investigate the effect of chitosan concentration on nanoparticle size during the reduction using a silver ion precursor. The second is to assess the antibacterial activity of the optimal nanocomposite as a mobile phone glass protector coating against Gram-positive *S. aureus* and Gram-negative *E. coli* at contact times of 24 and 48 h.

2. EXPERIMENTAL METHODS

2.1. Materials. Silver nitrate ($AgNO_3$) solids (99.0% purity, Sigma-Aldrich, St. Louise, Missouri) were used as precursor materials for the synthesis of the metal nanoparticle. Through a local supplier, the following reagents were purchased: high-molecular-weight (HMW) chitosan powder (≥75% degree of deacetylation, Sigma-Aldrich, St. Louise, Missouri), glacial acetic acid solution (Ajax, Sydney, Australia), and anhydrous sodium hydroxide pellets (≥97% purity, HiMedia, Mumbai, India). The glass protectors used were Samsung A12 camera lens glass protectors with dimensions 2.5 cm × 2.5 cm purchased from a local store in Cebu, Philippines.

The bacterial cultures that were used for the antibacterial assay were *S. aureus* and *E. coli*. These were grown in nutrient broth and agar. Saline solution (0.9% w/v sodium chloride in distilled water) was used as a dilution and recovery medium during the assay.

2.2. Sterilization of Apparatus, Glassware, Films, and Workplace. Prior to the coating procedures and the antibacterial assay, sterilization procedures were conducted. This step is vital to all microbial studies to prevent contamination by unwanted pathogens.

Glass protectors and apparatuses (such as Petri dishes, forceps, and pipette tips) used in the coating procedures were sterilized in an autoclave at 121 °C for 15 min. They were kept wrapped and covered prior to use. On the other hand, apparatuses (such as Petri dishes, culture tubes, forceps, inoculation loops, and pipettes) used in the antibacterial assay were decontaminated in an autoclave at 121 °C for 30 min. These were then cleaned with liquid soap, rinsed with tap water, and then rinsed with distilled water. Once dried, they were wrapped with thick paper and sterilized again at 170 °C for 120 min. These were also kept covered prior to use. The workplace surface was wiped with a disinfectant solution and then with 70% isopropyl alcohol. The room was thoroughly cleaned and sprayed with disinfectant spray.

For the duration of the experiments, aseptic techniques were also practiced. Mainly, these were (1) proper use of sterile gloves, (2) regular hand disinfection, (3) torching of forceps in between the handling of different samples, (4) limiting the exposure of media to open air (i.e., keeping Petri dishes and culture tubes containing media closed when not in use), and (5) keeping apparatuses covered prior to use.

2.3. Synthesis of ChAgNPs. Glacial acetic acid (1% w/v) was used to dissolve HMW chitosan powder to obtain 0.1, 0.2, 0.4, 0.6, and 0.8% w/v chitosan solutions. The prepared solutions were then transferred to an Erlenmeyer flask and agitated for 1 h at 40 °C in an incubator shaker at a speed of 150 rpm. The solution was then cooled to ambient temperature before the conduct of reduction synthesis.

The reduction of silver ions to silver nanoparticles using chitosan was adapted from the modified experimental procedures by Kalaivani et al. and by Dara et al.[37,38] Five milliliters (5 mL) of the prepared $AgNO_3$ solution and two milliliters (2 mL) of freshly prepared 0.1 M NaOH solution were added to the chitosan solution. The prepared samples were then agitated in an incubator shaker for 6 h at 70 °C and 150 rpm. The prepared samples were transferred to amber bottles and stored in a dark, ambient area to mitigate photooxidation.

2.4. Particle Imaging and Size Analysis. Five milliliter aliquots of each produced concentration sample were obtained from the ChAgNP solution samples produced. The samples were sonicated at a frequency of 35 Hz for 10 min and were diluted at a 1:1 ratio with deionized water to mitigate interference of the polymeric material to the electron beam, which can cause unviewable images upon microscopy. The diluted samples were drop-cast onto a Ted Pella 01811 C/B 200 mesh Cu film and air-dried. Later, the dried cast films were viewed under a JEOL JEM-2100F field emission transmission electron microscope (FE-TEM) at 200 volts and a magnification of ×150,000.

The generated TEM image of each sample was then subjected to image processing using *ImageJ* software for the determination of diameter size measurement as performed in previous studies on nanocomposite particles.[39,40] The expected image must result in a scale of 1:50 nm. The recorded data for each sample were then evaluated in a normal distribution, and the average nanoparticle diameter and standard deviation were calculated.

Based on the results, a selection among the produced ChAgNPs was done. Based on the trend from size imaging, the obtained samples were examined to check whether the average nanoparticle size falls within the definitive nanoparticle size range of 1 to 100 nm. The optimal formulation was then used for further characterization using UV−vis spectroscopy, Fourier transfer infrared (FTIR) spectroscopy, and ζ-potential.

2.5. Nanoparticle Presence and Optical Properties via UV−Vis Spectroscopy. The ChAgNP nanocomposite at optimal chitosan concentration was examined under a UV−vis absorbance spectrometer (SHIMADZU UV-1900i, Japan). Aliquots of the optimal formulation, the one with 0.8% w/v chitosan concentration, were placed in a 1 cm quartz cuvette. Spectroscopy was done at a spectrum of range of 200−900 nm and was performed under ambient temperature.

2.6. Chemical Bond Composition via FTIR. FTIR analysis was used to confirm the identity of the nanocomposite by identifying the presence of molecular bonds in the formation of the nanocomposite. Further investigation was made under a diffused reflective FTIR (Perkin Elmer spectrum 100, USA) with attenuated total reflectance (ATR). The sample was studied such that the spectrum ran at 10 scans, with each scan running in the range of 4000−600 cm^{-1} with a resolution of 0.09 cm^{-1}. The liquid sample was deposited using a dropper and was not dried prior. After each use, hexane was used to clean the sample surface.

https://doi.org/10.1021/acsomega.3c00191
ACS Omega 2023, 8, 17699−17711

2.7. ζ-Potential and Particle Size Distribution via Dynamic Light Scattering (DLS). The optimal formulation was further examined for particle size distribution and ζ-potential using the nanoPartica SZ-100 (Horiba Ltd, Japan) equipment operated with a voltage range of −200 to +200 mV. The sonicated sample was injected into a disposable carbon-coated cell with a volume of 100 μL in which the device measures the electrophoretic mobility of the particle surface. The sample was exposed to about 25 °C and at 90° scattering angle.

2.8. Application of ChAgNPs on Glass Protectors. Eight (8) commercial mobile phone glass protectors (2.5 cm × 2.5 cm) were used per coating material used. Another eight mobile phone glass protectors were used as blank (uncoated) samples. The thickness of the glass was measured using a handheld thickness gauge (Mitutoyo, Japan) with a resolution of 0.01 mm. The procedure was adapted from the American Society for Testing and Materials (ASTM) Standards D1005: Procedure C for handheld micrometers.

To measure the thickness of the uncoated tempered glass, the anvil was allowed to be in contact with the substrate, without compressing it, by rotating the adjustment knob. The thickness of the tempered glass was read from the four corners of the panel and on the center. Three trials of thickness measurements were done for each substrate, and the average was calculated.

A modified method of Bormashenko et al. and Chandren & Zulfemi was used in the drop-casting procedure of this study.[41,42] Glass protectors were then placed on a flat surface. The optimum ChAgNP formulation was cast by dropping a 1 mL solution onto the glass substrate. The pipette was positioned at around 15 cm above the glass substrate. Then, the four corners and the center of the glass substrate were dropped with the ChAgNPs. The substrate was left to dry at room temperature. To ensure the adhesion of the ChAgNP coating onto the glass surface, a physical curing method was adapted from Vieira et al.[43] The coated tempered glass was oven-dried at 50 °C for 12 h or overnight.

The coated samples were measured for their thickness, following the same procedures done for the uncoated glass protectors. The difference between the coated and uncoated samples is the thickness of the nanocomposite on the glass substrate.

2.9. Antibacterial Assay. The antibacterial assay is meant to assess the antibacterial activity of the ChAgNP coating by finding the log reduction of the number of bacteria on the coated surface after a specific contact time (i.e., duration of time the glass is in contact with the bacteria). A modified version of the ISO 22196 with changes from Campos et al.,[44] who investigated film screen protectors instead of glass, was adapted. This method is designed to quantitatively evaluate the ability of a plastic or nonporous surface to inhibit growth or to kill bacteria. It is usually done over a 24 h contact time but could be modified to other periods according to study objectives. Currently, this is the most popular test protocol for testing the antibacterial activity of a surface.[44]

The optimal ChAgNP coating (with the smallest mean particle diameter) was evaluated for antibacterial activity at different contact times (24 and 48 h). The bacteria evaluated were Gram-positive *S. aureus* and Gram-negative *E. coli*. The positive infection control was represented by uncoated glass surfaces. Samples and control were evaluated in triplicates.

To prepare the culture broth, 13 g of nutrient broth powder was dissolved per 1 L of distilled water. To prepare the agar, 28 g of nutrient agar powder was dissolved per 1 L of distilled water. The solution was mixed well and then sterilized by autoclaving at 121 °C for 15 min. The resulting liquid agar was poured into a Petri dish and solidified. Bacterial cultures of *E. coli* and *S. aureus* were streaked onto plated nutrient agar and incubated for 24 h at 37 °C for colonies to grow. The resulting cultures were then collected using inoculation loops to make 10 mL bacterial suspensions with a cell density of 1.5×10^8 CFU/mL according to the 0.5 McFarland standard. This was the target cell density for sample contact.

The 10 mL bacterial suspensions were poured each into a Petri dish. The glass protectors were each placed and soaked in the Petri dish for bacterial contact. This is a modification from ISO 22196, which proposed that bacterial contact be done with inoculation of the culture onto the surface and with the use of a plastic film for covering. The samples were then incubated at 37 °C to encourage growth.

After a certain contact time (24 and 48 h) at 37 °C, the glass surfaces were each submerged in 0.9% w/v sodium chloride solution in a Petri dish. The glass protectors were agitated in solution for 30 s. One mL of each resulting solution was serially diluted 10-fold until 10^{-6}. Twenty μL of the culture solutions in the dilutions of 10^4, 10^5, and 10^6 were plated and then incubated for 24 h at 37 °C.

After incubation, a total plate count was performed on all plated samples. From here, the CFU per plate (U_t and A_t) was calculated. The antibacterial activity was measured in terms of the log reduction of the number of bacteria (in colony-forming units or CFU) on the test sample compared to that of the positive infection control (uncoated surface). This calculation for the antibacterial activity R_t is represented by eq 1 as adapted from ISO 22196. The CFU values to be used in the computations were the mean average of plate counts. There were two different contact times at which the antibacterial activity was measured.

$$R_t = (U_t - A_t) \times 100\% \quad (1)$$

such that U_t = mean common logarithm of CFU of positive infection control after a time. A_t = mean common logarithm of CFU of sample after a time

3. RESULTS AND DISCUSSION

3.1. Synthesis of ChAgNPs. Figure 1 shows the appearance of each ChAgNP composite setup. The difference

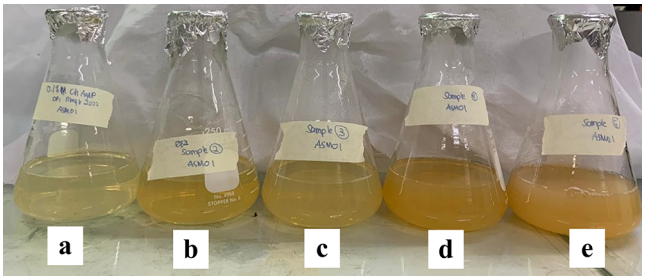

Figure 1. Visual appearance of ChAgNP samples after reduction and stabilization of silver nitrate solution to metal nanoparticles with chitosan solution at varied concentrations of (a) 0.1% w/v, (b) 0.2% w/v, (c) 0.4% w/v, (d) 0.6% w/v, and (e) 0.8% w/v, with the addition of NaOH and agitation at 70 °C, 150 rpm for 6 h.

https://doi.org/10.1021/acsomega.3c00191
ACS Omega 2023, 8, 17699−17711

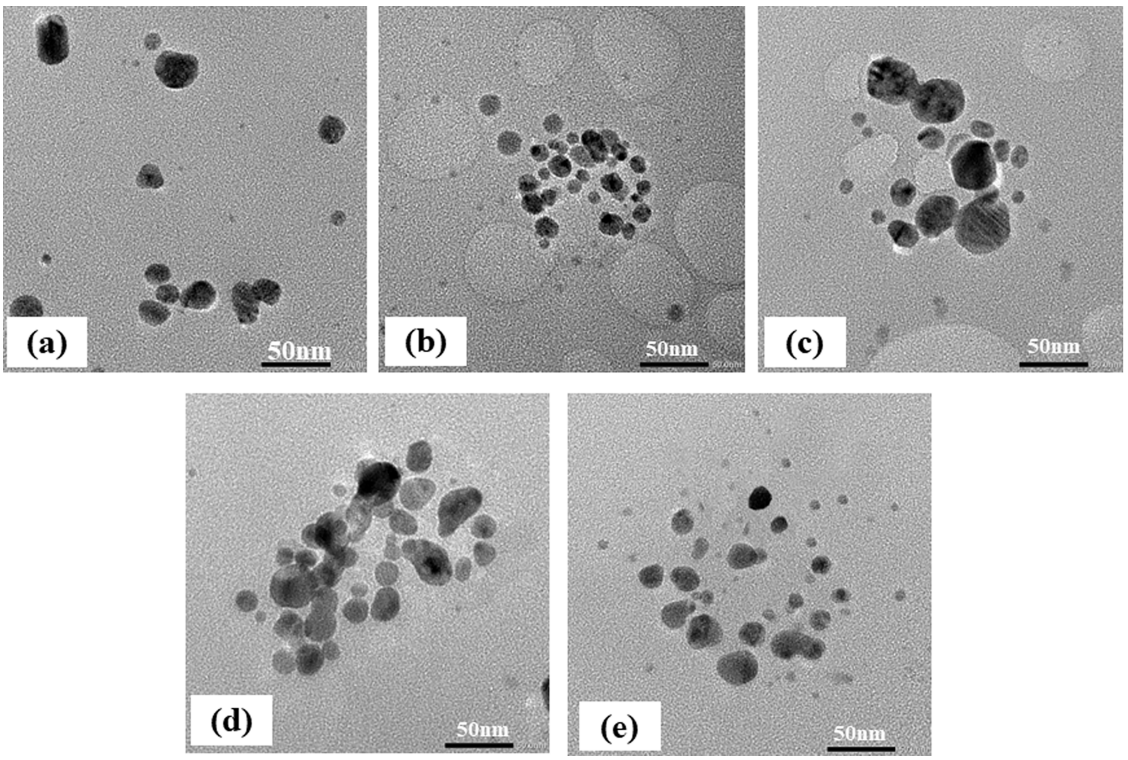

Figure 2. TEM images of chitosan-silver nanoparticles at varied chitosan solution concentrations: (a) 0.1% w/v, (b) 0.2% w/v, (c) 0.4% w/v, (d) 0.6% w/v, and (e) 0.8% w/v.

in color is attributed to the variations in the concentration of the chitosan solution added. The amounts of $AgNO_3$ and of NaOH solutions were kept constant among samples. Different concentrations of chitosan solution (i.e., 0.1, 0.2, 0.4, 0.6, 0.8% w/v) were used in the synthesis of silver nanoparticles. Upon preparation, the chitosan solution used was very little, and the resulting solution was soluble, and no solid clumps were observed after incubation shaking. During synthesis, a color change to yellow to yellow-brown signifies the presence of ChAgNPs. Such an observation is an indication of the formation of silver nanoparticles.[32,38,45,46]

3.2. Particle Size Analysis and Determination of Optimal ChAgNP Formulation. The synthesized samples were observed under a transmission electron microscope (TEM), which shows a two-dimensional magnified image of the nanocomposite. The TEM images revealed AgNPs in black quasi-spherical nanostructures. From the generated images, it could be seen that the sizes of the nanoparticles decrease as the concentration of the chitosan increases. The TEM images were viewed using the bright-field configuration.

Different concentrations of chitosan solution (i.e., 0.1, 0.2, 0.4, 0.6, 0.8% w/v) were used in the synthesis of silver nanoparticles. The TEM images revealed AgNPs in black quasi-spherical nanostructures. From the generated images, it could be seen that the sizes of the nanoparticles decrease as the concentration of the chitosan increases. The TEM images were viewed using the bright-field configuration. As seen in Figure 2, some areas of the sample tend to appear darker than the other areas. In the bright-field imaging, the transmitted electron beam is selected with the aperture, and the scattered electrons are blocked. Consequently, areas with crystalline or high mass materials will tend to appear dark in the image. This is due to the fact that heavier materials scatter electrons more intensely than do the lighter ones.[47]

Figure 3 presents the particle size distribution determined from each sample. The graph shows the particle range as well

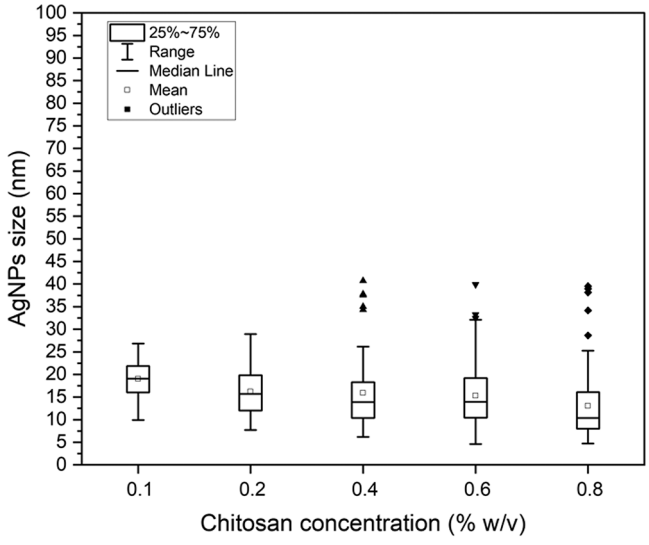

Figure 3. Box and whisker plot for the particle size distribution of chitosan-silver nanoparticles at varied chitosan solution concentrations.

as the outliers. The presence of outliers could be a possible indication of the presence of agglomeration occurring in the solution. In 0.1% w/v chitosan, the particle diameters were in the range of 8.09−29.42 nm with a mean diameter of 19.05 ± 4.15 nm. For 0.2% w/v chitosan, the particle diameters fell in the range of 7.73−28.91 nm with a mean diameter of 16.15 ±

https://doi.org/10.1021/acsomega.3c00191
ACS Omega 2023, 8, 17699−17711

Scheme 1. Mechanism of the Synthesis of ChAgNPs Using Chitosan Solution as Reducing and Capping Agents at the Conditions Used in the Experimental Method

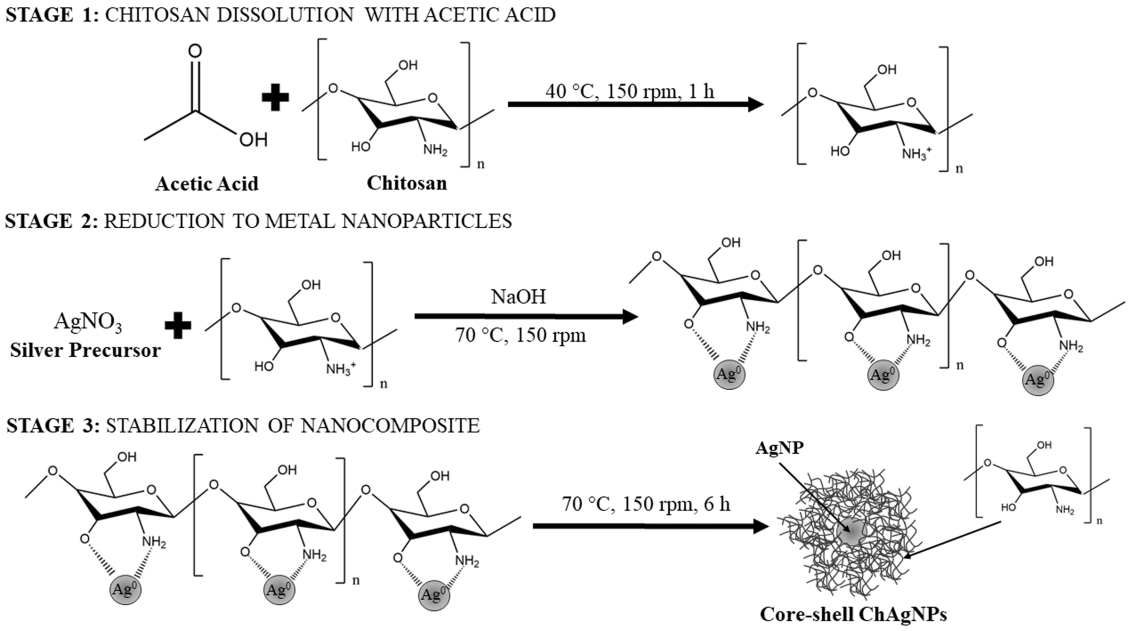

6.02 nm. The particle diameters of ChAgNPs using 0.4% w/v chitosan were in the range of 5−45 nm with a mean diameter of 15.91 ± 7.67 nm. The sample with 0.6% w/v chitosan has particle diameters ranging from 4.59 to 39.92 nm with a mean diameter of 15.30 ± 6.99 nm. Last, the sample using 0.8% w/v chitosan has a measured particle diameter range of 4.09−34.91 nm with a mean diameter of 13.98 ± 5.54 nm.

The decreasing size of the silver nanoparticles with increasing chitosan concentration was consistent with the hypothesis of Phan et al. such that the size of the metal nanoparticles is greatly influenced by the concentration of chitosan.[16] The correlation of the chitosan concentration and the metal nanoparticle size can be attributed to the strong interaction between the positively charged chitosan and the metal nuclei. This interaction results in the inhibition of the binding precursors to the metal nuclei, which then results in the inhibition of the metal nuclei growth. TEM images show few to no aggregation between synthesized ChAgNPs, which implies repulsion of the nanocomposite particles to prevent aggregation. These repulsions were attributed to the electrostatic interaction between the polymeric chitosan-silver composites, creating a steric barrier with a positive charge density covering the metal core.[16]

Scheme 1 shows the possible mechanism of the synthesis of the nanocomposite, which includes reduction and stabilization through the chitosan solution. Ag^+ ions were reduced to Ag^0 with chitosan. Such a mechanism is attributed to the presence of free electrons provided by the oxidation of alcohols or glucoside groups in the chitosan molecule. The synthesis of ChAgNPs was also achieved within 6 h due to the increased temperature of 70 °C, which allowed the reduction reaction to occur faster. Another possible explanation for the reduction reaction was the presence of amine groups. Chitosan contains amine groups, which also helped in the reduction of silver ions to silver nanoparticles. Amines are a popular class of organic compounds due to their universal presence in several biological and environmental systems and processes.[39,48] Amine-containing polysaccharides such as chitosan have been reported to act as dual reductants and capping agents. During the formation of ChAgNPs, the primary amine and its nearby hydroxyl group in the chitosan structure enable the reduction of the positively charged silver ions to form silver metal.[49] In addition, polymeric amines were also reported to have growth-limiting capabilities and prevent agglomeration of the metallic nanoparticles by creating a matrix around the metal nanoparticle, forming the nanocomposite.[17] The capping of the resulting agglomeration through bonding with chitosan allows the AgNPs to have a controlled size.

3.3. Characterization of Optimal ChAgNP Nanocoating. Further characterization procedures were conducted to assess the chemical composition and stability of the nanocomposite at the optimal conditions. These subsections show the results of the UV−vis spectroscopy, Fourier transfer infrared (FTIR) spectroscopy, particle size, and ζ-potential of the nanocomposite and their implications toward the attributes of the produced mixture.

3.3.1. UV−Vis Spectroscopy. Figure 4 shows the UV−vis spectroscopy of the optimal formulation of ChAgNPs (i.e., using 0.8% w/v chitosan solution). Along with this spectrum plot are two other spectrum plots of the used chitosan solution and of a chemically synthesized AgNP solution using 0.1 M silver nitrate and trisodium citrate dihydrate (TSC) adapted from the procedures done by Yerragopu et al.[45]

As observed in the spectra, the ChAgNP plot has absorption peaks at 236 and 261 nm. It also displays an increase in absorption from 700 nm until it reaches around 261 nm. The values in the wavelength range of 200−219 nm were omitted in this plot as they yielded unwanted fluctuations or noise, making them insignificant to the plot. When compared to the literature, there is an observed shift of wavelength from the expected peak points to the actual results despite similarities in trend.[32,37,38] Usually, the expected peak of produced ChAgNPs falls at around 350−410 nm. However, as seen in Figure 4, the peaks are seen at 236 and 261 nm, while a slight rise with the peak at about 422 nm can be observed. The peak at 236 nm is consistent with the peak of the chitosan solution plot (in

https://doi.org/10.1021/acsomega.3c00191
ACS Omega 2023, 8, 17699−17711

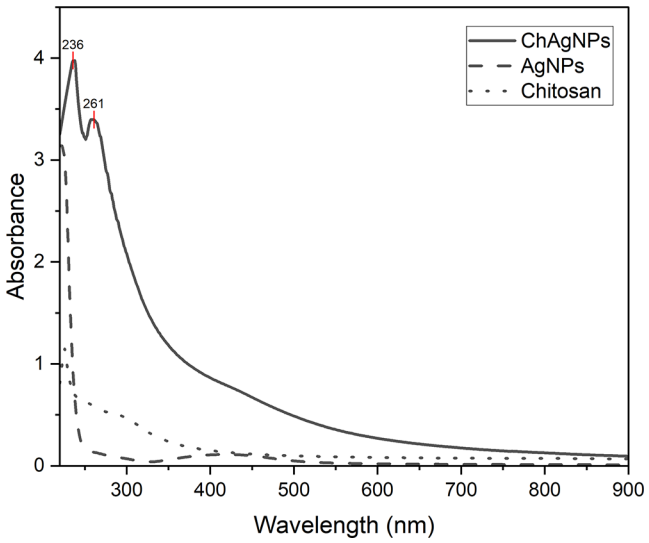

Figure 4. UV−vis absorbance plot of ChAgNPs using 0.8% w/v chitosan solution (in bold), AgNPs using TSC (in dash) and 0.8% w/v chitosan solution (in dash-dot) at the wavelength range of 220−900 nm.

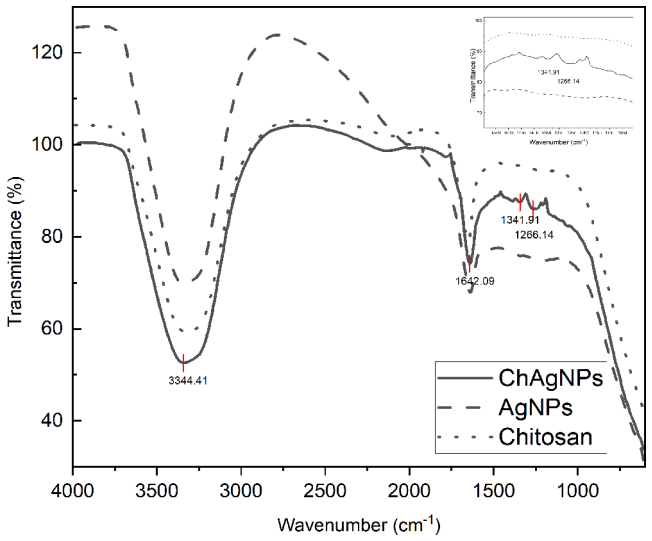

Figure 5. FTIR analysis result of ChAgNPs (in bold), AgNPs using trisodium citrate (in dash), and 0.8% w/v chitosan solution (in dash-dot) from 4000 to 600 cm^{-1} with the inset plot (upper right corner) in the wavenumber range from 1525 to 1025 cm^{-1}.

dotted lines), while the slight rise at 422 nm is similar to the rise observed in the AgNP plot at the same wavelength.

The observed peaks in the ChAgNP plot, in comparison to the AgNP and chitosan plots, imply that the nanocomposite is present. Also, possible nanoclusters of Ag ions (Ag^{+} and $[Ag_2]^{2+}$) may be present in the nanocomposite based on the absorbance peak at 261 nm.[50,51] Also, the absorbance reading measured in the plot is significant to the turbidity of the nanocomposite solution upon application onto glass protectors such that a high absorbance value implies a more intense color of the coating.

3.3.2. Fourier Transform Infrared Spectroscopy (FTIR). Through Fourier transform infrared spectroscopy, the organic and inorganic species in a sample can be identified based on its absorbance of infrared light. Chemical bonds interact with light by stretching, contracting, and bending. A chemical bond absorbs infrared light at a specific range of wavenumber, allowing for the determination of the functional groups present.[52]

Figure 5 presents the transmittance (%) versus wavenumber (cm^{-1}) plot of the synthesized ChAgNPs. The numerical labels shown within the plot give the spectrum peaks, bends, and stretches detected by the spectrometer. Along with the figure are two other FTIR plots of synthesized AgNPs using TSC and of 0.8% w/v chitosan solution.

In the ChAgNP plot, a stretched peak at 3344.41 cm^{-1} implies the presence of an aliphatic primary amine. Another implication is that a normal hydroxyl (−OH) bond exists in the nanocomposite since the stretch at that point is estimated at about 3400−3200 cm^{-1}.[53] This peak is consistent with both chitosan and AgNP plots, yet the variation of this peak with the other plots can be attributed to the reduction and stabilization of the nanocomposite.[32] Another significant point observed is a bended point at 1642.09 cm^{-1}, which implies the presence of the secondary amine, similar to the studies conducted by Nate et al.[23] and Govindan et al.[54] Unique to the ChAgNP plot in comparison to the AgNP and the chitosan plots are its fingerprint peaks found in wavenumbers 1341.91 and 1247.20 cm^{-1}. In the inset of Figure 5 is a zoomed FTIR plot in the wavenumber range of 1500−1100 cm^{-1} where these fingerprint peaks were observed. Notice in the inset plot that these peaks occur after the oxidation of chitosan with silver ions, compared to the chitosan FTIR plot. These peaks represent the presence of a tertiary amine, similar to the observations of Govindan[54] in his method of producing ChAgNPs. It may also be suspected that these peaks can be attributed to the presence of alkyl groups, in the case of the 1247.20 cm^{-1} peak, and carboxylic groups from the acetic acid for the 1341.91 cm^{-1} peak. It can be implied that an oxidation of chitosan occurred through the interaction of its amine bonds with the reduced silver. This reaction results in a tertiary amine in the chitosan structure.

3.3.3. ζ-Potential of the Optimal Nanocomposite Formulation. ζ-Potential is a quantification of the effective electric charge that surrounds the surface of the nanocomposite. It measures the difference between the oppositely charged ions on the nanocomposite surface and the bulk fluid where the dispersion of the nanocomposite takes place. This electric charge plays a huge role in the stability behavior and toxicity of the nanomaterial.[55]

The optimal formulation is further assessed by its ζ-potential and particle size distribution. In this analysis, a dynamic light scattering (DLS) zetasizer was used to determine the particle size distribution and ζ-potential of the optimal formulation.

Shown in Table 1 is the result of the particle size analysis and ζ-potential of the optimal nanocomposite formulation using the said equipment on a per-trial basis. Along with the

Table 1. Particle Size (PS) and ζ-Potential (ZP) Analyses of the Optimal ChAgNP Formulation

	particle size (nm)		ζ-potential (mV)
trial	mean	standard deviation	mean
1	178.6	70.3	+52.7
2	180.8	83.8	+57.8
3	187.9	91.4	+53.2
average	182.4	81.8	+54.6

https://doi.org/10.1021/acsomega.3c00191
ACS Omega 2023, 8, 17699−17711

same table is the average of the three trials. The average ζ-potential of the ChAgNPs, derived from 30 runs per concentration sample, was above +54.6 mV. Such a result is a very high value showing a very stable nanoparticle in the dispersive medium. Such a ζ-potential shows that a high aggregative stability exists due to the strong repulsive forces in the nanocomposite. The usual indication of a stable nanocomposite is a ζ-potential that exceeds at around +25 to +30 mV or −25 to −30 mV.[50]

A particle size analysis was done on the optimum sample to determine the overall average size of the nanocomposite. As shown in Table 1, the average nanocomposite size is 182.4 nm. The mean value was significantly higher than the nanocomposite particle diameter value from the TEM imaging and size distribution (Figure 3), which was 13.98 nm. The difference of the measured sizes is the chitosan layer that capped the silver nanoparticles. Dynamic light spectrophotometry has been noted to capture both the nanocomposite particle and the capping layer, as seen also in a previous study by Tan and Lee[56] on metal/polymeric nanocomposite particles. The particle size distribution of the optimum sample, shown in Figure 6, exhibits a distribution curve skewed to the

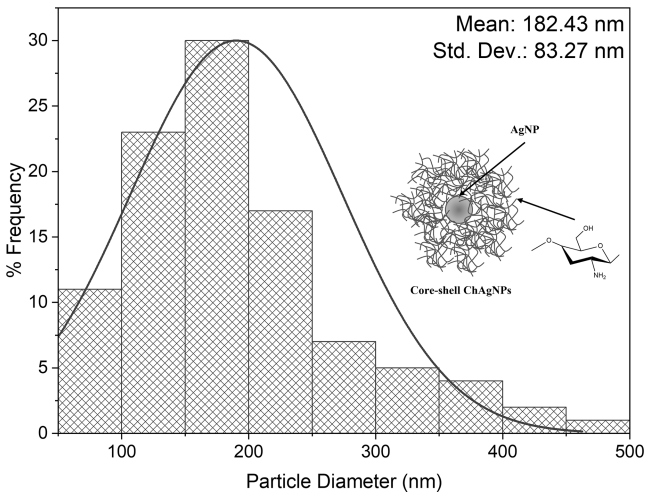

Figure 6. Particle size distribution of optimum ChAgNPs using 0.8% w/v chitosan solution.

left. The particle size analysis results show that the synthesized nanocomposite has both a silver nanoparticle (core) and the chitosan (shell), which functions as the capping agent or stabilizer. The TEM image was not able to depict the chitosan layer of the nanocomposite. The observed particles under the TEM were only the AgNPs because the sample was previously dried before the TEM imaging. Hence, the electron beam that passes through the sample under TEM viewing may have destroyed the chitosan layer, making it invisible on the TEM image. Bita et al. investigated the effects of electron beams on hydroxyapatite/chitosan composite (MgHApCs) coatings. The study reported that an unirradiated layer of the sample can produce clear and smooth images, and the pattern of polymeric molecules is clearly visible. However, when electron beams were passed through the sample upon SEM viewing, differences in the morphology and topography of the surfaces of MgHApCs coatings were observed. It was observed that there was a shrinkage in the polymer content from the sample layers. Several SEM images were taken to show the effects of the electron beam on polymeric samples, and it was observed that, when an electron beam is passed through the sample, the polymeric layers of the sample gradually detach from the substrate.[57]

3.4. Coating of ChAgNP Nanocomposite on Glass Screen Protectors. The application of chitosan-silver nanocomposite as an antibacterial coating on mobile phone glass protectors was carried out through the drop-casting method. This method is a simple and low-cost deposition method for film coating. Unlike spray-coating and dip-coating techniques, the drop-casting method is a facile and a more controllable coating technique. In addition, controlling the repeatability and uniformity of the spray-on films is reported to be difficult. According to Eslamian & Soltani-Kordshuli, if the coating application is limited to a small-area thin solid film, the drop-casting method is the most appropriate. Drop-casting depends on the release of large droplets that spread and wet the surface upon impact.[42,58] Different studies have also reported the effectiveness of the drop-casting technique in the polymer coating application on glass substrates.[59−61]

AgNPs synthesized using TSC and 0.8% w/v chitosan solutions were also used in the coating application of mobile phone glass protectors. The coated glass protectors were air-dried for 2 h at room temperature and then placed in an oven at 50 °C for 12 h to facilitate the curing process.

After the coating and curing process, glasses of different coating solutions were observed to have different colors, as shown in Figure 7. The glasses that were coated with the

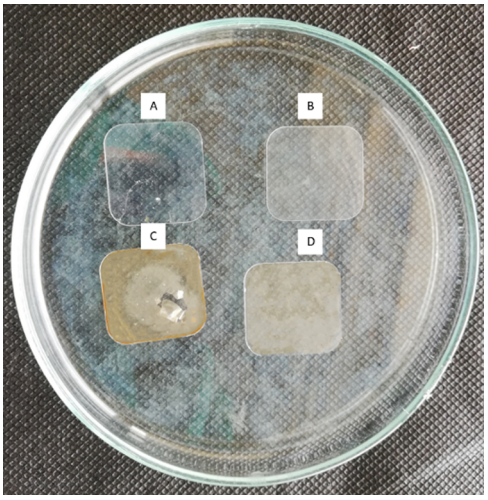

Figure 7. Tempered glass screen protectors coated with different coating solutions: (A) no coating, (B) AgNPs, (C) ChAgNPs (using 0.8% w/v chitosan solution), and (D) 0.8% w/v chitosan solution.

ChAgNP solution have a very thin light-brown layer on the coated face (Figure 7c), and those that were coated by the 0.8% w/v chitosan solution have a faint yellow layer of coating (Figure 7d). On the other hand, the samples that were coated by the chemically synthesized silver nanoparticles have a layer of cloudy white coating (Figure 7b). Finally, the uncoated glass panel is clear and transparent (Figure 7a).

Only a few studies on the application of chitosan-silver nanoparticles as coatings for mobile phone glass protectors are currently available. The successful coating of ChAgNPs could be attributed to the adhesion of the synthesized nanoparticles on the glass surface. This phenomenon can be explained by the adhesion theory by Joo & Baldwin.[62] The adhesive adhesion

https://doi.org/10.1021/acsomega.3c00191
ACS Omega 2023, 8, 17699−17711

theory states that two surfaces, upon close contact with each other, have mechanical interlocking and physical adsorption where intermolecular forces such as the van der Waals interaction between parallel surfaces and that chemical bond would take place. Another possible explanation could be from the particle adhesion theory. In this theory, the conceptual mechanism of interaction is attributed to the van der Waals and chemical bonds. In the particle adhesion theory, such an interaction occurs between a flat surface (glass) and spherical particles (ChAgNPs). Thus, the possibility of adhesion contact area between the nanoparticle and the glass substrate could be linked to the intermolecular and intramolecular bonds in which the long-range and short-range forces are in action.

However, as a coating for mobile phone screens, ChAgNPs may alter the screen color of phones due to the yellow-brown pigmentation that exists in the nanocomposite solution. The turbidity of the coating can also be observed from the UV−vis plot, shown in Figure 4, in which high absorbance was obtained at certain wavelengths, indicating the strong presence of color in the material. Although its aim is to provide antibacterial protection, the aesthetic aspect of using the nanocomposite coating is currently at a disadvantage.

3.5. Antibacterial Assay of ChAgNPs on Glass Protectors. ChAgNPs on glass protectors were evaluated for antibacterial activity at different contact times (24 and 48 h). A modified version of ISO 22196 (measurement of antibacterial activity on plastics and other nonporous surfaces) was used. Some procedures from Campos et al.[44] who investigated film screen protectors instead of glass were adapted. For comparison, AgNPs using TSC as well as 0.8% w/v chitosan solution (Ch) were investigated using the same antibacterial assay procedures.

Table 2 presents the antibacterial activities of ChAgNPs, AgNPs, and Ch on glass protectors against Gram-negative *E. coli* and Gram-positive *S. aureus* after contact times of 24 and 48 h. These two bacterial species are popular representative strains for each of the two types of bacteria.[63]

Table 2. Antibacterial Activity of ChAgNP Synthesized with 0.8% w/v Chitosan Solution Coated on Glass, AgNP, and 0.8% Chitosan Solution against *E. coli* and *S. aureus* after 24 and 48 h

bacteria	*E. coli*		*S. aureus*	
contact time (h)	24 h	48 h	24 h	48 h
treatment	antibacterial activity (%)			
ChAgNP	49.80	32.60	none[b]	none[b]
AgNP	70.51	maximum[a]	27.98	none[b]
Ch	50.01	31.33	31.16	none[b]

[a]Maximum = %log reduction is equal to or exceeded 100%. [b]None = bacterial growth or no reduction of bacteria was observed.

ChAgNPs performed near similarly with Ch against *E. coli* after both 24 h (49.80 and 50.01%, respectively) and 48 h (32.60 and 31.33%, respectively), while AgNPs exhibited the greatest antibacterial activity against *E. coli* at both contact times. At 48 h, it performed a maximum log reduction of colony-forming units. Chitosan performed the best out of the three treatments against *S. aureus* at 24 h (31.16%). Antibacterial disparity between ChAgNPs and Ch is also better seen against *S. aureus*. ChAgNPs failed to reduce *S. aureus* at both contact times.

The antibacterial activity of ChAgNPs is reduced at a longer contact time. This is also observable in most other cases. The only exception is AgNPs against *E. coli* at 48 h whose antibacterial activity increased after 24 h. It is also worth noting that minimal to no studies have been done on the antibacterial activity of ChAgNPs coated on glass surfaces or on any of the present study's specimens on glass surfaces beyond 24 h. To the best of our knowledge, this is the first time the chitosan-derived silver nanoparticle as nanocoating is used as an antibacterial solution on mobile phone glass protectors.

Despite being a nanocomposite of both Ch and silver, the antibacterial activity of ChAgNP is mostly attributed to the latter component. Chitosan in ChAgNP mostly serves as the reducing and stabilizing agent and the biopolymer matrix in which the AgNPs are contained.[64−67] In a Kirby−Bauer test where inhibition of bacterial growth around the test surface is observed, only Ch (T3) exhibited very minimal antimicrobial activity against both *E. coli* and *S. aureus* as evidenced by the presence of bacterial colonies around the perimeter of the Ch glass protectors. On the contrary, ChAgNP (T1) and AgNP (T2) visibly have microbial inhibition as revealed by the clear outline surrounding the perimeter of the T1 and T2 glasses. The Kirby−Bauer test is pictured in Figure 8. Due to the nature of the test, this may also be indicative of the inability of Ch to diffuse around its surface area unlike the silver nanoparticles in ChAgNP and AgNP.

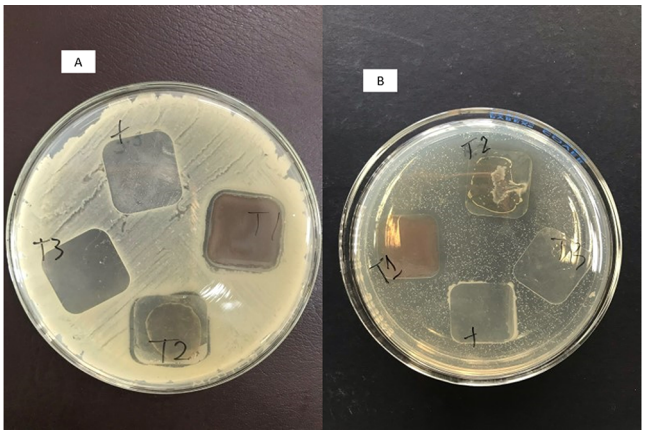

Figure 8. Kirby−Bauer test on (+) positive infection control, (T1) ChAgNP, (T2) AgNP, and (T3) Ch against (A) *E. coli* and (B) *S. aureus* after 24 h of incubation at 37 °C.

All three treatments performed better against *E. coli* than against *S. aureus*. In fact, after 48 h against *S. aureus*, all three failed to reduce bacteria on the surface. Both ChAgNP and AgNP particularly exhibited comparatively higher antibacterial activity against *E. coli*. Silver nanoparticles are mostly active against Gram-negative bacteria such as *E. coli* and *P. aeruginosa* and are comparatively less active in reducing Gram-positive *S. aureus*.[68−70] This immunity by Gram-positive bacteria is due to the thicker cell wall, about 10 times more than that of Gram-negative bacteria, with multiple murein layers and teichoic acid.[68,69] This higher susceptibility of *E. coli* than of *S. aureus* against silver has also been observed in another investigation involving AgNP on glass surfaces.[63]

AgNPs have been known to show antibacterial activity in many studies. The mechanism of their interaction with

https://doi.org/10.1021/acsomega.3c00191
ACS Omega 2023, 8, 17699−17711

bacterial cells has also been a popular topic in the literature, and discussions have rarely been consistent. One proposition states that AgNPs are merely sources of silver ions and therefore deposit these onto the cell wall where they adhere to the cytoplasmic membrane.[71,72] Silver ions are said to cause the disruption of enzymatic activity and, occasionally, to cell death through their reaction with the thiol groups of the protein molecules.[71] Some investigations have revealed that the antibacterial activity has more to do with the AgNPs themselves. AgNPs are larger in size than silver ions, allowing them to react with more molecules and thus exhibit greater antimicrobial activity.[70] They are said to accumulate on the cell wall and membrane and cause disruptive morphological changes to the cell as shown both in scanning electron microscopy (SEM) and in transmission electron microscopy (TEM) studies.[73,74] The antibacterial effect may also have been due to the AgNPs and the silver ions.[19] Regardless, AgNPs and silver ions, being of silver, are possibly said to react with the sulfur and phosphorus of the bacterial deoxyribonucleic acid (DNA). This mechanism interferes with DNA replication and cell reproduction and may even cause the death of the microorganism itself.[72,75]

In comparison to TSC-synthesized AgNPs, ChAgNPs do not exhibit an improved antibacterial performance. The apparent underperformance in the antibacterial activity of ChAgNP versus AgNP, especially in nonporous or glass applications, cannot very well yet be explained by the existing literature. Such an underperformance may be due to the biopolymer nature of chitosan. Biopolymers are said to encourage growth and persistence of bacteria even under unfavorable conditions.[70,76] This is, however, in contradiction to the many studies that have proven the antibacterial activity of chitosan.[77−79] It may be then that a combination of the application type and of the interaction between chitosan and silver leads to a reduced antibacterial activity of ChAgNPs.

The current use of an alcohol sanitizer spray is arguably the most popular disinfection method for mobile phone screens. However, its antibacterial property is not embedded in the glass itself. Rather, disinfection occurs only as often as the user remembers to perform it. Otherwise, the bacteria remain and cultivate on the glass surface, increasing the risk of fomite transmission. On the other hand, the antibacterial activity of an embedded coating is constant, and the antibacterial activity begins as soon as bacteria land on the glass surface.

4. CONCLUSIONS AND RECOMMENDATIONS

The study shows affirmative results on the relationship between an increase in chitosan concentration and the decrease in nanocomposite diameter. All five samples at varied chitosan concentrations (0.1, 0.2, 0.4, 0.6, and 0.8% w/v) are within the specified nanometer range based on their average diameters of AgNPs measured from TEM images.

Based on the data collected from size distribution, the ChAgNPs produced with a formulation of 0.8% w/v chitosan concentration were selected as the smallest of the group. Further characterization using FTIR and UV−vis spectroscopy plots on the selected optimal formulation shows a positive indication of the presence of ChAgNPs. In terms of its ζ-potential, the optimal formulation yielded an average of +54.6 mV, implying high aggregating stability in the nanocomposite. Further studies can be developed in terms of how chitosan acts as a reducing and capping agent in the synthesis of the nanocomposite.

The glasses that were coated with the ChAgNP solution with the smallest particle diameter have a very thin, light-brown layer on the coated face. There was no significant difference between the thickness of the glass before and after it was coated. Moreover, ChAgNP as a glass coating exhibits antibacterial activity against *E. coli* for up to 48 h of contact. However, the antibacterial activity decreases from 24 h (49.80%) to 48 h (32.60%). No antibacterial activity by ChAgNP on glass was observed against *S. aureus*.

Further studies on the application of ChAgNP as an antibacterial coating on glass are recommended. For one, there should be investigations on other materials or component materials that can synergistically interact with ChAgNPs to develop an improved antibacterial coating material. Another proposition is to explore a "smart" ChAgNP-based antibacterial coating. Second, the mechanism of antibacterial action of the material, the interactions between chitosan and silver in the nanocomposite, and the effects of such interactions on antibacterial activity must be investigated. The results of this study can hopefully encourage the development of a green-synthesized nanocomposite glass coating that can exhibit significant antibacterial activity. In terms of thickness, a higher resolution should be used to obtain a more accurate and precise measurement of the thickness of the coating layer.

AUTHOR INFORMATION

Corresponding Author

Noel Peter Tan − *Department of Chemical Engineering, College of Technology and Center for Advanced New Materials, Engineering, and Emerging Technologies (CANMEET), University of San Agustin, Iloilo City 5000, Philippines;* Present Address: Member, Engineering & Industrial Research Division, National Research Council of the Philippines (NRCP); Present Address: Balik-Scientist Program (BSP), Philippine Council for Industry, Energy, and Emerging Technology Research and Development, Department of Science and Technology, Taguig, Philippines; orcid.org/0000-0002-5424-9616; Email: dtan@usa.edu.ph, noelpetert@gmail.com

Authors

Gibson Jake C. Canama − *Department of Chemical Engineering, University of San Carlos, Cebu City 6000, Philippines*

Monica Claire L. Delco − *Department of Chemical Engineering, University of San Carlos, Cebu City 6000, Philippines*

Rhoel A. Talandron − *Department of Chemical Engineering, University of San Carlos, Cebu City 6000, Philippines*

Complete contact information is available at: https://pubs.acs.org/10.1021/acsomega.3c00191

Author Contributions

The manuscript was written through contributions of all authors. All authors have given approval to the final version of the manuscript. These authors contributed equally.

Notes

The authors declare no competing financial interest.

https://doi.org/10.1021/acsomega.3c00191
ACS Omega 2023, 8, 17699−17711

■ ACKNOWLEDGMENTS

The authors would like to acknowledge the support provided by the Department of Science and Technology-Science Education Institute (DOST-SEI) Merit Scholarship and the National Research Council of the Philippines (NRCP), and to the University of San Carlos Department of Chemical Engineering, to the Department of Science and Technology-Industrial Technology Development Institute (TEM imaging), to Sigmatech, Inc. (DLS equipment), to the University of San Carlos Department of Chemistry (FTIR), and to the University of San Carlos Department of Biology (Antibacterial Assay) for the use of their equipment and facilities.

■ ABBREVIATIONS

ChAgNP/s, chitosan-silver nanoparticles/nanocomposites; AgNP/s, silver nanoparticles

■ REFERENCES

(1) Bhoonderowa, A.; Gookool, S.; Biranjia-Hurdoyal, S. D. The Importance of Mobile Phones in the Possible Transmission of Bacterial Infections in the Community. *J. Community Health* **2014**, *39*, 965−967.

(2) Akinyemi, K. O.; Atapu, A. D.; Adetona, O. O.; Coker, A. O. The Potential Role of Mobile Phones in the Spread of Bacterial Infections. *J. Infect. Dev. Countries* **2009**, *3*, 628−632.

(3) Ulger, F.; Dilek, A.; Esen, S.; Sunbul, M.; Leblebicioglu, H. Are Healthcare Workers' Mobile Phones a Potential Source of Nosocomial Infections? Review of the Literature. *J. Infect. Dev. Countries* **2015**, *9*, 1046−1053.

(4) Kramer, A.; Schwebke, I.; Kampf, G. How Long Do Nosocomial Pathogens Persist on Inanimate Surfaces? A Systematic Review. *BMC Infect. Dis.* **2006**, *6*, 130.

(5) Dastider, D.; Jyoti Sen, D.; Kumar Mandal, S.; Bose, S.; Ray, S.; Mahanti, B. Hand Sanitizers Bid Farewell To Germs on Surface Area of Hands. *Eur. J. Pharm. Med. Res.* **2020**, *7*, 648−656.

(6) Pereira, S.; Esparza, J.; Leroux, P. Scratch Resistance of Cell Phone Screen Protectors. technical report, Nanovea, 2019, .

(7) De Jong, B.; Meeder, A. M.; Koekkoek, K. W. A. C.; Schouten, M. A.; Westers, P.; van Zanten, A. R. H. Pre−Post Evaluation of Effects of a Titanium Dioxide Coating on Environmental Contamination of an Intensive Care Unit: The Titanic Study. *J. Hosp. Infect.* **2018**, *99*, 256−262.

(8) Govind, V.; Bharadwaj, S.; Sai Ganesh, M. R.; Vishnu, J.; Shankar, K. V.; Shankar, B.; Rajesh, R. Antiviral Properties of Copper and Its Alloys to Inactivate Covid-19 Virus: A Review. *Biometals* **2021**, *34*, 1217−1235.

(9) Ketchel, M. Copper is great at killing superbugs − so why don't hospitals use it? The Conversation. https://theconversation.com/copper-is-great-at-killing-superbugs-so-why-dont-hospitals-use-it-73103 (accessed 2021-09-17).

(10) Sánchez-López, E.; Gomes, D.; Esteruelas, G.; Bonilla, L.; Lopez-Machado, A. L.; Galindo, R.; Cano, A.; Espina, M.; Ettcheto, M.; Camins, A.; Silva, A. M.; Durazzo, A.; Santini, A.; Garcia, M. L.; Souto, E. B. Metal-Based Nanoparticles as Antimicrobial Agents: An Overview. *Nanomaterials* **2020**, *10*, 292.

(11) Salleh, A.; Naomi, R.; Utami, N. D.; Mohammad, A. W.; Mahmoudi, E.; Mustafa, N.; Fauzi, M. B. The Potential of Silver Nanoparticles for Antiviral and Antibacterial Applications: A Mechanism of Action. *Nanomaterials* **2020**, *10*, 1566.

(12) Vanamu, E.; Ene, M.; Biţă, B.; Ionescu, C.; Crăciun, L.; Sârbu, I. In Vitro Human Microbiota Response to Exposure to Silver Nanoparticles Biosynthesized with Mushroom Extract. *Nutrients* **2018**, *10*, 607.

(13) Dallas, P.; Sharma, V. K.; Zboril, R. Silver Polymeric Nanocomposites as Advanced Antimicrobial Agents: Classification, Synthetic Paths, Applications, and Perspectives. *Adv. Colloid Interface Sci.* **2011**, *166*, 119−135.

(14) Sen, I. K.; Mandal, A. K.; Chakraborti, S.; Dey, B.; Chakraborty, R.; Islam, S. S. Green Synthesis of Silver Nanoparticles Using Glucan from Mushroom and Study of Antibacterial Activity. *Int. J. Biol. Macromol.* **2013**, *62*, 439−449.

(15) Anastas, P. T.; Zimmerman, J. B. *Innovations in Green Chemistry and Green Engineering*; Springer Science+Business Media: New York, 2013.

(16) Phan, T. T. V.; Phan, D. T.; Cao, X. T.; Huynh, T. C.; Oh, J. Roles of Chitosan in Green Synthesis of Metal Nanoparticles for Biomedical Applications. *Nanomaterials* **2021**, *11*, 273.

(17) Seltenrich, N. Nanosilver: Weighing the Risks and Benefits. *Environ. Health Perspect.* **2013**, *121*, a220.

(18) Hofmeister, H.; Tan, G. L.; Dubiel, M. Shape and Internal Structure of Silver Nanoparticles Embedded in Glass. *J. Mater. Res.* **2005**, *20*, 1551−1562.

(19) Pallavicini, P.; Dacarro, G.; Taglietti, A. Self-Assembled Monolayers of Silver Nanoparticles: From Intrinsic to Switchable Inorganic Antibacterial Surfaces. *Eur. J. Inorg. Chem.* **2018**, *2018*, 4846−4855.

(20) Iravani, S.; Korbekandi, H.; Mirmohammadi, S. V.; Zolfaghari, B. Synthesis of Silver Nanoparticles: Chemical, Physical and Biological Methods. *Res. Pharm. Sci.* **2014**, *9*, 385.

(21) Gudikandula, K.; Maringanti, S. C. Synthesis of Silver Nanoparticles by Chemical and Biological Methods and Their Antimicrobial Properties. *J. Exp. Nanosci.* **2016**, *11*, 714−721.

(22) Huang, H.; Yang, X. Synthesis of Chitosan-Stabilized Gold Nanoparticles in the Absence Presence of Tripolyphosphate. *Biomacromolecules* **2004**, *5*, 2340−2346.

(23) Nate, Z.; Moloto, M. J.; Mubiayi, P. K.; Sibiya, P. N. Green Synthesis of Chitosan Capped Silver Nanoparticles and Their Antimicrobial Activity. *MRS Adv.* **2018**, *3*, 2505−2517.

(24) Nisha, V.; Monisha, C.; Ragunathan, R.; Johney, J. Use of Chitosan as Edible Coating on Fruits and in Micro Biological Activity-An Ecofriendly Approach. *Int. J. Pharm. Sci. Invent.* **2016**, *5*, 7−14.

(25) Salgado-Cruz, M. d. l. P.; Salgado-Cruz, J.; García-Hernández, A. B.; Calderón-Domínguez, G.; Gómez-Viquez, H.; Oliver-Espinoza, R.; Fernández-Martínez, M. C.; Yáñez-Fernández, J. Chitosan as a Coating for Biocontrol in Postharvest Products: A Bibliometric Review. *Membranes* **2021**, *11*, 421.

(26) Regiel, A.; Irusta, S.; Kyzioł, A.; Arruebo, M.; Santamaria, J. Preparation and Characterization of Chitosan-Silver Nanocomposite Films and Their Antibacterial Activity against Staphylococcus Aureus. *Nanotechnology* **2013**, *24*, No. 015101.

(27) Qi, L.; Xu, Z.; Jiang, X.; Hu, C.; Zou, X. Preparation and Antibacterial Activity of Chitosan Nanoparticles. *Carbohydr. Res.* **2004**, *339*, 2693−2700.

(28) Moodley, J. S.; Krishna, S. B. N.; Pillay, K.; Sershen; Govender, P. Green Synthesis of Silver Nanoparticles from Moringa Oleifera Leaf Extracts and Its Antimicrobial Potential. *Adv. Nat. Sci.: Nanosci. Nanotechnol.* **2018**, *9*, No. 015011.

(29) Kumar, S.; Mukherjee, A.; Dutta, J. Chitosan Based Nanocomposite Films and Coatings: Emerging Antimicrobial Food Packaging Alternatives. *Trends Food Sci. Technol.* **2020**, *97*, 196−209.

(30) (a) Rahman, A.; Kumar, S.; Bafana, A.; Dahoumane, S. A.; Jeffryes, C. Biosynthetic Conversion of Ag+ to Highly Stable Ag0 Nanoparticles by Wild Type and Cell Wall Deficient Strains of Chlamydomonas Reinhardtii. *Molecules* **2019**, *24*, 98.

(31) Rao, M. D.; Pennathur, G. Green Synthesis and Characterization of Cadmium Sulphide Nanoparticles from Chlamydomonas Reinhardtii and Their Application as Photocatalysts. *Mater. Res. Bull.* **2017**, *85*, 64−73.

(32) Venkatesham, M.; Ayodhya, D.; Madhusudhan, A.; Veerababu, N.; Veerabhadram, G. A Novel Green One-Step Synthesis of Silver Nanoparticles Using Chitosan: Catalytic Activity and Antimicrobial Studies. *Appl. Nanosci.* **2014**, *4*, 113−119.

(33) Martínez-Castañón, G. A.; Niño-Martínez, N.; Martínez-Gutierrez, F.; Martínez-Mendoza, J. R.; Ruiz, F. Synthesis and Antibacterial Activity of Silver Nanoparticles with Different Sizes. *J. Nanopart. Res.* **2008**, *10*, 1343−1348.

https://doi.org/10.1021/acsomega.3c00191
ACS Omega 2023, 8, 17699−17711

(34) Sirelkhatim, A.; Mahmud, S.; Seeni, A.; Kaus, N. H. M.; Ann, L. C.; Bakhori, S. K. M.; Hasan, H.; Mohamad, D. Review on Zinc Oxide Nanoparticles: Antibacterial Activity and Toxicity Mechanism. *Nano-Micro Lett.* **2015**, *7*, 219−242.
(35) Raghupathi, K. R.; Koodali, R. T.; Manna, A. C. Size-Dependent Bacterial Growth Inhibition and Mechanism of Antibacterial Activity of Zinc Oxide Nanoparticles. *Langmuir* **2011**, *27*, 4020−4028.
(36) West, A. M.; Teska, P. J.; Lineback, C. B.; Oliver, H. F. Strain, Disinfectant, Concentration, and Contact Time Quantitatively Impact Disinfectant Efficacy. *Antimicrob. Resist. Infect. Control* **2018**, *7*, No. 49.
(37) Dara, P. K.; Mahadevan, R.; Digita, P. A.; Visnuvinayagam, S.; Kumar, L. R. G.; Mathew, S.; Ravishankar, C. N.; Anandan, R. Synthesis and Biochemical Characterization of Silver Nanoparticles Grafted Chitosan (Chi-Ag-NPs): In Vitro Studies on Antioxidant and Antibacterial Applications. *SN Appl. Sci.* **2020**, *2*, No. 665.
(38) Kalaivani, R.; Maruthupandy, M.; Muneeswaran, T.; Hameedha Beevi, A.; Anand, M.; Ramakritinan, C. M.; Kumaraguru, A. K. Synthesis of Chitosan Mediated Silver Nanoparticles (Ag NPs) for Potential Antimicrobial Applications. *Front. Lab. Med.* **2018**, *2*, 30−35.
(39) Tan, N. P. B.; Lee, C. H.; Chen, L.; Ho, K. M.; Lu, Y.; Ballauff, M.; Li, P. Facile Synthesis of Gold/Polymer Nanocomposite Particles Using Polymeric Amine-Based Particles as Dual Reductants and Templates. *Polymer* **2015**, *76*, 271−279.
(40) Tan, N. P. B. Novel Metal/Core-Shell Polymer Composite Particles: Synthesis, Characterization and Potential Applications, The Hong Kong Polytechnic University, 2014. https://theses.lib.polyu.edu.hk/handle/200/7746 (accessed 2023-03-31).
(41) Chandren, S.; Zulfemi, N. H. Titania Nanoparticles Coated on Polycarbonate Car Headlights for Self-Cleaning Purpose. *J. Phys.: Conf. Ser* **2019**, *1321*, No. 022032.
(42) Bormashenko, E.; Bormashenko, Y.; Frenkel, M. Formation of Hierarchical Porous Films with Breath-Figures Self-Assembly Performed on Oil-Lubricated Substrates. *Materials* **2019**, *12*, 3051.
(43) Vieira, M. L. G.; Esquerdo, V. M.; Nobre, L. R.; Dotto, G. L.; Pinto, L. A. A. Glass Beads Coated with Chitosan for the Food Azo Dyes Adsorption in a Fixed Bed Column. *J. Ind. Eng. Chem.* **2014**, *20*, 3387−3393.
(44) Campos, M. D.; Zucchi, P. C.; Phung, A.; Leonard, S. N.; Hirsch, E. B. The Activity of Antimicrobial Surfaces Varies by Testing Protocol Utilized. *PLoS One* **2016**, *11*, No. e0160728.
(45) Yerragopu, P. S.; Hiregoudar, S.; Nidoni, U.; Ramappa, K. T.; Sreenivas, A. G.; Doddagoudar, S. R. Chemical Synthesis of Silver Nanoparticles Using Tri-Sodium Citrate, Stability Study and Their Characterization. *Int. Res. J. Pure Appl. Chem.* **2020**, 37−50.
(46) Chowdhury, S.; Yusof, F.; Faruck, M. O.; Sulaiman, N. Process Optimization of Silver Nanoparticle Synthesis Using Response Surface Methodology. *Procedia Eng.* **2016**, *148*, 992−999.
(47) Gaston, B.; Han, L. TEM: Bright field versus dark field - Chemistry LibreTexts. CHEMISTRY LibreTexts. https://chem.libretexts.org/Courses/Franklin_and_Marshall_College/Introduction_to_Materials_Characterization__CHM_412_Collaborative_Text/Electron_and_Probe_Microscopy/TEM%3A_Bright_field_versus_dark_field (accessed 2022-08-19).
(48) Newman, J. D. S.; Blanchard, G. J. Formation of Gold Nanoparticles Using Amine Reducing Agents. *Langmuir* **2006**, *22*, 5882−5887.
(49) (a) Sonseca, A.; Madani, S.; Rodríguez, G.; Hevilla, V.; Echeverría, C.; Fernández-García, M.; Muñoz-Bonilla, A.; Charef, N.; López, D. Multifunctional PLA Blends Containing Chitosan Mediated Silver Nanoparticles: Thermal, Mechanical, Antibacterial, and Degradation Properties. *Nanomaterials* **2019**, *10*, 22.
(50) Ozin, G. A.; Hugues, F. S. Silver Atoms and Small Silver Clusters Stabilized in Zeolite Y: Optical Spectroscopy. *J. Phys. Chem. A* **1983**, *87*, 94−97.
(51) Ma, R.; Zhao, J.; Chen, X.; Qiao, X.; Fan, X.; Du, J.; Zhang, X. Stabilization of Ultra-Small [Ag2]2+ and [Agm]N+ Nano-Clusters through Negatively Charged Tetrahedrons in Oxyfluoride Glass Networks: To Largely Enhance the Luminescence Quantum Yields. *Phys. Chem. Chem. Phys.* **2017**, *19*, 22638−22645.
(52) Tan, N. P. B. Novel Metal/Core-Shell Polymer Composite Particles: Synthesis, Characterization and Potential Applications. 2014.
(53) Nandiyanto, A. B. D.; Oktiani, R.; Ragadhita, R. How to Read and Interpret FTIR Spectroscope of Organic Material. *Indones. J. Sci. Technol.* **2019**, *4*, 97−118.
(54) Govindan, S.; Nivethaa, E. A. K.; Saravanan, R.; Narayanan, V.; Stephen, A. Synthesis and Characterization of Chitosan-Silver Nanocomposite. *Appl. Nanosci.* **2012**, *2*, 299−303.
(55) Lowry, G. V.; Hill, R. J.; Harper, S.; Rawle, A. F.; Hendren, C. O.; Klaessig, F.; Nobbmann, U.; Sayre, P.; Rumble, J. Guidance to Improve the Scientific Value of Zeta-Potential Measurements in NanoEHS. *Environ. Sci. Nano* **2016**, *3*, 953−965.
(56) Tan, N. P. B.; Lee, C. H. Environment-Friendly Approach in the Synthesis of Metal/ Polymeric Nanocomposite Particles and Their Catalytic Activities on the Reduction of p-Nitrophenol to p-Aminophenol. *Green Chem. Process. Synth.* **2017**. DOI: 10.5772/INTECHOPEN.68388.
(57) Bita, B.; Stancu, E.; Stroe, D.; Dumitrache, M.; Ciobanu, S. C.; Iconaru, S. L.; Predoi, D.; Groza, A. The Effects of Electron Beam Irradiation on the Morphological and Physicochemical Properties of Magnesium-Doped Hydroxyapatite/Chitosan Composite Coatings. *Polymers* **2022**, *14*, 582.
(58) Eslamian, M.; Soltani-Kordshuli, F. Development of Multiple-Droplet Drop-Casting Method for the Fabrication of Coatings and Thin Solid Films. *J. Coat. Technol. Res.* **2018**, *15*, 271−280.
(59) Cheng, Y.; Wu, B.; Ma, X.; Lu, S.; Xu, W.; Szunerits, S.; Boukherroub, R. Facile Preparation of High Density Polyethylene Superhydrophobic/Superoleophilic Coatings on Glass, Copper and Polyurethane Sponge for Self-Cleaning, Corrosion Resistance and Efficient Oil/Water Separation. *J. Colloid Interface Sci.* **2018**, *525*, 76−85.
(60) Esteves, A. C. C.; Luo, Y.; Van De Put, M. W. P.; Carcouët, C. C. M.; De With, G. Self-Replenishing Dual Structured Superhydrophobic Coatings Prepared by Drop-Casting of an All-in-One Dispersion. *Adv. Funct. Mater.* **2014**, *24*, 986−992.
(61) Melavanki, R.; Vaijayanthimala, S.; Yallur, B. C.; Shelar, V. M.; Singh, D.; Sadasivuni, K. K.; Patil, N. R. Preparation and Optical Parameter Characterization of Two Aldehyde Derivative Thin Films for Photonic Applications by Drop Casting Method. *Luminescence* **2020**, *35*, 903−912.
(62) Joo, S.; Baldwin, D. F. Adhesion Mechanisms of Nanoparticle Silver to Substrate Materials: Identification. *Nanotechnology* **2010**, *21*, No. 055204.
(63) Pallavicini, P.; Taglietti, A.; Dacarro, G.; Antonio Diaz-Fernandez, Y.; Galli, M.; Grisoli, P.; Patrini, M.; Santucci De Magistris, G.; Zanoni, R. Self-Assembled Monolayers of Silver Nanoparticles Firmly Grafted on Glass Surfaces: Low Ag+ Release for an Efficient Antibacterial Activity. *J. Colloid Interface Sci.* **2010**, *350*, 110−116.
(64) López-Carballo, G.; Higueras, L.; Gavara, R.; Hernández-Muñoz, P. Silver Ions Release from Antibacterial Chitosan Films Containing in Situ Generated Silver Nanoparticles. *J. Agric. Food Chem.* **2013**, *61*, 260−267.
(65) Kumar-Krishnan, S.; Prokhorov, E.; Hernández-Iturriaga, M.; Mota-Morales, J. D.; Vázquez-Lepe, M.; Kovalenko, Y.; Sanchez, I. C.; Luna-Bárcenas, G. Chitosan/Silver Nanocomposites: Synergistic Antibacterial Action of Silver Nanoparticles and Silver Ions. *Eur. Polym. J.* **2015**, *67*, 242−251.
(66) Paulkumar, K.; Gnanajobitha, G.; Vanaja, M.; Pavunraj, M.; Annadurai, G. Green Synthesis of Silver Nanoparticle and Silver Based Chitosan Bionanocomposite Using Stem Extract of Saccharum Officinarum and Assessment of Its Antibacterial Activity. *Adv. Nat. Sci.: Nanosci. Nanotechnol.* **2017**, *8*, No. 035019.

https://doi.org/10.1021/acsomega.3c00191
ACS Omega 2023, 8, 17699−17711

(67) Raghavendra, G. M.; Jung, J.; kim, D.; Seo, J. Microwave Assisted Antibacterial Chitosan-Silver Nanocomposite Films. *Int. J. Biol. Macromol.* **2016**, *84*, 281−288.
(68) Greulich, C.; Braun, D.; Peetsch, A.; Diendorf, J.; Siebers, B.; Epple, M.; Köller, M. The Toxic Effect of Silver Ions and Silver Nanoparticles towards Bacteria and Human Cells Occurs in the Same Concentration Range. *RSC Adv.* **2012**, *2*, 6981−6987.
(69) Amato, E.; Diaz-Fernandez, Y. A.; Taglietti, A.; Pallavicini, P.; Pasotti, L.; Cucca, L.; Milanese, C.; Grisoli, P.; Dacarro, C.; Fernandez-Hechavarria, J. M.; Necchi, V. Synthesis, Characterization and Antibacterial Activity against Gram Positive and Gram Negative Bacteria of Biomimetically Coated Silver Nanoparticles. *Langmuir* **2011**, *27*, 9165−9173.
(70) Ghosh, S.; Patil, S.; Ahire, M.; Kitture, R.; Kale, S.; Pardesi, K.; Cameotra, S.; Bellare, J.; Dhavale, D. D.; Jabgunde, A.; Chopade, B. A. Synthesis of Silver Nanoparticles Using Dioscorea Bulbifera Tuber Extract and Evaluation of Its Synergistic Potential in Combination with Antimicrobial Agents. *Int. J. Nanomed.* **2012**, 483−496.
(71) Belusso, L. C. S.; Lenz, G. F.; Fiorini, E. E.; Pereira, A. J.; Sequinel, R.; Bini, R. A.; Felix, J. F.; Schneider, R. Synthesis of Silver Nanoparticles from Bottom up Approach on Borophosphate Glass and Their Applications as SERS, Antibacterial and Glass-Based Catalyst. *Appl. Surf. Sci.* **2019**, *473*, 303−312.
(72) Yin, I. X.; Zhang, J.; Zhao, I. S.; Mei, M. L.; Li, Q.; Chu, C. H. The Antibacterial Mechanism of Silver Nanoparticles and Its Application in Dentistry. *Int. J. Nanomed.* **2020**, *15*, 2555−2562.
(73) Sondi, I.; Salopek-Sondi, B. Silver Nanoparticles as Antimicrobial Agent: A Case Study on E. Coli as a Model for Gram-Negative Bacteria. *J. Colloid Interface Sci.* **2004**, *275*, 177−182.
(74) Raffi, M.; Mahmood Bhatti, T.; Akhter, J. I.; Hameed, A. Antibacterial Characterization of Silver Nanoparticles against *E. Coli* ATCC-15224. *J. Mater. Sci. Technol.* **2008**, *24*, 192−196.
(75) Ahamed, M.; AlSalhi, M. S.; Siddiqui, M. K. J. Silver Nanoparticle Applications and Human Health. *Clin. Chim. Acta* **2010**, *411*, 1841−1848.
(76) Moradali, M. F.; Rehm, B. H. A. Bacterial Biopolymers: From Pathogenesis to Advanced Materials. *Nat. Rev. Microbiol.* **2020**, *18*, 195.
(77) No, H. K.; Young Park, N.; Ho Lee, S.; Meyers, S. P. Antibacterial Activity of Chitosans and Chitosan Oligomers with Different Molecular Weights. *Int. J. Food Microbiol.* **2002**, *74*, 65−72.
(78) Li, J.; Zhuang, S. Antibacterial Activity of Chitosan and Its Derivatives and Their Interaction Mechanism with Bacteria: Current State and Perspectives. *Eur. Polym. J.* **2020**, *138*, No. 109984.
(79) Arkoun, M.; Ardila, N.; Heuzey, M. C.; Ajji, A. *Chitosan-Based Structures/Coatings with Antibacterial Properties*; Elsevier Inc., 2017. DOI: 10.1016/B978-0-12-811982-2.00017-2.

https://doi.org/10.1021/acsomega.3c00191
ACS Omega 2023, 8, 17699−17711